J|A|C|S ARTICLES

Published on Web 09/25/2009

K3 Fragment of Amyloidogenic β_2-Microglobulin Forms Ion Channels: Implication for Dialysis Related Amyloidosis

Mirela Mustata,[†] Ricardo Capone,[†] Hyunbum Jang,[‡] Fernando Teran Arce,[†] Srinivasan Ramachandran,[†] Ratnesh Lal,*[,†] and Ruth Nussinov*[,‡,§]

Center for Nanomedicine and Department of Medicine, University of Chicago, Chicago, Illinois 60637, Center for Cancer Research Nanobiology Program, NCI-Frederick, SAIC-Frederick, Inc., Frederick, Maryland 21702, and Sackler Institute of Molecular Medicine, Department of Human Genetics and Molecular Medicine, Sackler School of Medicine, Tel Aviv University, Tel Aviv 69978, Israel

Received June 19, 2009; E-mail: ruthnu@helix.nih.gov; rlal@uchicago.edu

Abstract: β_2-microglobulin (β_2m) amyloid deposits are linked to dialysis-related amyloidosis (DRA) in hemodialysis patients. The mechanism by which β_2m causes DRA is not understood. It is also unclear whether only the full-length β_2m induces pathophysiology or if proteolytic fragments are sufficient for inducing this effect. Ser20-Lys41 (K3) is a digestion fragment of full-length β_2m. Solid state NMR (ssNMR) combined with X-ray diffraction and atomic force microscopy (AFM) revealed the characteristic oligomeric amyloid conformation of the U-turn *β-strand-turn-β-strand* motif stacked in parallel and stabilized by intermolecular interactions also shown by $A\beta_{9-40}$/$A\beta_{17-42}$ and the CA150 WW domain. Here we use the K3 U-turn atomic coordinates and molecular dynamic (MD) simulations to model K3 channels in the membrane. Consistent with previous AFM imaging of other amyloids that show channel-like structures in the membrane, in the simulations K3 also forms ion channels with 3−6 loosely attached mobile subunits. We carry out AFM, single channel electrical recording, and fluorescence imaging experiments. AFM images display 3D ion channel topography with shapes, morphologies, and dimensions consistent with the theoretical model. Electrical conductance measurements indicate multiple single channel conductances, suggesting that various K3 oligomer sizes can constitute the channel structure. Fluorescence measurements in kidney cells show channel-mediated cell calcium uptake. These results suggest that the β_2m-induced DRA can be mediated by ion channels formed by its K3 fragment. Because the *β-strand-turn-β-strand* motif appears to be a universal amyloid feature, its ability to form ion channels further suggests that the motif may play a generic role in toxicity.

Introduction

Beta-2-microglobulin (β_2m), a 99 residue component of the major histocompatibility complex class I (MHC-1) contains seven β-strands arranged as a β-sandwich with one intramolecular disulfide bond.[1] In the normal catabolic process, β_2m is degraded and excreted by the kidneys. In long-term renal dialysis patients, due to the impermeability of the artificial dialysis membrane to β_2m, it accumulates in the blood with levels increasing up to 50−100 fold. The high concentration of β_2m leads to pathogenic fibril formations resulting in dialysis related amyloidosis (DRA).[2] The mechanisms by which β_2m causes DRA and whether a full-length[3,4] is required for the disorder or truncated β_2m[5−7] is sufficient are still unclear.

Full-length β_2m forms amyloid-like fibrils.[8,9] Fragments of β_2m can also form fibrils with distinct morphologies under different conditions[10−13] and even shorter fragments (6 residues)

[†] University of Chicago.
[‡] SAIC-Frederick, Inc.
[§] Tel Aviv University.

(1) Trinh, C. H.; Smith, D. P.; Kalverda, A. P.; Phillips, S. E.; Radford, S. E. *Proc. Natl. Acad. Sci. U.S.A.* **2002**, *99*, 9771–9776.
(2) Radford, S. E.; Gosal, W. S.; Platt, G. W. *Biochim. Biophys. Acta* **2005**, *1753*, 51–63.
(3) Gejyo, F.; Yamada, T.; Odani, S.; Nakagawa, Y.; Arakawa, M.; Kunitomo, T.; Kataoka, H.; Suzuki, M.; Hirasawa, Y.; Shirahama, T.; Cohen, A. S.; Schmid, K. *Biochem. Biophys. Res. Commun.* **1985**, *129*, 701–706.
(4) Gorevic, P. D.; Casey, T. T.; Stone, W. J.; DiRaimondo, C. R.; Prelli, F. C.; Frangione, B. *J. Clin. Inves.t* **1985**, *76*, 2425–2429.
(5) Linke, R. P.; Hampl, H.; Bartel-Schwarze, S.; Eulitz, M. *Biol. Chem. Hoppe Seyler* **1987**, *368*, 137–144.
(6) Linke, R. P.; Hampl, H.; Lobeck, H.; Ritz, E.; Bommer, J.; Waldherr, R.; Eulitz, M. *Kidney Int.* **1989**, *36*, 675–681.
(7) Esposito, G.; Michelutti, R.; Verdone, G.; Viglino, P.; Hernandez, H.; Robinson, C. V.; Amoresano, A.; Dal Piaz, F.; Monti, M.; Pucci, P.; Mangione, P.; Stoppini, M.; Merlini, G.; Ferri, G.; Bellotti, V. *Protein Sci.* **2000**, *9*, 831–845.
(8) Jahn, T. R.; Tennent, G. A.; Radford, S. E. *J. Biol. Chem.* **2008**, *283*, 17279–17286.
(9) Eakin, C. M.; Berman, A. J.; Miranker, A. D. *Nat. Struct. Mol. Biol.* **2006**, *13*, 202–208.
(10) Gosal, W. S.; Morten, I. J.; Hewitt, E. W.; Smith, D. A.; Thomson, N. H.; Radford, S. E. *J. Mol. Biol.* **2005**, *351*, 850–864.
(11) Hasegawa, K.; Ohhashi, Y.; Yamaguchi, I.; Takahashi, N.; Tsutsumi, S.; Goto, Y.; Gejyo, F.; Naiki, H. *Biochem. Biophys. Res. Commun.* **2003**, *304*, 101–106.
(12) Ivanova, M. I.; Gingery, M.; Whitson, L. J.; Eisenberg, D. *Biochemistry* **2003**, *42*, 13536–13540.
(13) Jones, S.; Manning, J.; Kad, N. M.; Radford, S. E. *J. Mol. Biol.* **2003**, *325*, 249–257.

 10.1021/ja9049299 CCC: $40.75

of β_2m form needle-like morphologies.[14,15] While several regions exhibit an intrinsic propensity for aggregation, a single region of about 10 residues in length determines the rate of fibril formation.[16] Significantly, β_2m amyloid fibril formation does not directly relate to cell toxicity in DRA.

Hirakura and Kagan[17] reported that β_2m formed nonselective, long-lived, and voltage independent ion channels in planar phospholipid bilayers consistent with DRA pathophysiology. Because, in common with other amyloid channels,[18] the β_2m channel was inhibited by Congo red and zinc, they proposed that it consisted of a β-sheet aggregated state. Multiple single channel conductances suggested that various β_2m oligomers can form channel structures.

A 22-residue β_2m peptide (K3) corresponding to Ser20-Lys41 spontaneously forms amyloid fibrils under wide range of pH and solvent conditions.[19−21] Using combined solid-state NMR (ssNMR), X-ray fiber diffraction, and atomic force microscopy (AFM), Goto and co-workers recently derived the 3D structure of the K3 protofibril (PDB id: 2E8D).[22] K3 adopted the U-shaped *β-strand-turn-β-strand* motif in common with other amyloid peptides.[23−26] Using the ssNMR-based K3 peptide coordinates, we modeled the linear- and annular-like structures of the K3 in solution[27] using all-atom molecular dynamics (MD). We observed that linear-like K3 oligomers have two possible peptide organizations: single-layered parallel-stranded β-sheets and double-layered CN−NC (C and N being the C- and N-terminal β-strands, respectively) oligomers with parallel orientation within the sheets and antiparallel organization between sheets. However, no stable K3 oligomers with either single- or double-layered annular features were observed in solution. Structural analysis using replica exchange MD revealed that a β-hairpin structure is predicted for the β_2m fragment (83−99),[28] while the *β-strand-turn-β-strand* motif is marginally populated in solution.[29]

U-shaped motifs were first predicted by modeling of Aβ_{16-35};[30] they were observed in the ssNMR model of Aβ_{9-40};[25] the p3 (Aβ_{17-42}) peptide[24] and in the CA150 WW domain.[26] They appear to be a general feature of amyloid organization.[23] For Aβ_{9-42}/Aβ_{17-42}, they are predicted to form *dynamic* cation-permeating channels in the fluidic membrane.[31,32] Because K3 also presents a U-shaped motif, the question arises as to its ability to also form ion-conducting channels in the lipid bilayer. If that is the case, it may suggest that a U-shaped conformation could be a generic toxic channel motif and that it could play a role in β_2m DRA. In this study, we model the channel and complement the simulations by AFM, single channel conductance measurements in the bilayer and Ca^{2+} uptake in kidney cells. Our results indicate that the K3 fragment has biophysical properties similar to β_2m.[17]

Materials and Methods

Chemicals. *n*-Hexane, *n*-heptane, KCl, $ZnCl_2$, and Hepes were from Sigma-Aldrich (St Louis, MO). Lipids 1-palmitoyl-2-oleoyl-*sn*-glycero-3-phosphoethanolamine (POPE), 1-palmitoyl-2-oleoyl-*sn*-glycero-3-[phospho-*rac*-(1-glycerol)] (POPG), 1,2-dioleoyl-*sn*-glycero-3-phospho-L-serine (DOPS), and 1,2-dioleolyl-*sn*-glycero-3-phosphatidyl-choline (DOPC) were from Avanti Polar Lipids (Birmingham, AL). Human kidney proximal tubule cells (HK2) obtained from ATCC (Manassas, VA) and grown in KSFM enriched with EGF and BPE (catalog #17005042) and Fluo-4 NW calcium assay kit were from Invitrogen Corp. (Carlsbad, CA). K3 peptide, synthesized in Dr. Carl Saxinger's lab at NIH-NCI, was dissolved in 1% ammonium hydroxide to a 1 mg/mL concentration.

Molecular Dynamics (MD) Simulation. The monomer conformation of the K3 peptide (a 22-residue fragment Ser20-Lys41 from β_2m) was extracted from the NMR-based structure of K3 protofilaments.[22] The K3 channel modeling closely follows the protocol successfully used previously for the Aβ fragments.[31,32] Using all-atom molecular dynamics (MD) simulations, we extended the number of monomers to 24 and initially constructed the annular structure of K3 channel with two different topologies: NC*p*CN channel with charged pore and CN*p*NC channel with hydrophobic pore (Figure 1).

The initial channel is minimized with a rigid body motion for the peptides to enhance the formation of backbone hydrogen bonds (H-bonds) within the β-sheet. The minimized channel is next embedded in the DOPC bilayer. A unit cell containing two layers of lipids with almost 170 000 atoms is constructed. The lipid bilayers containing 340 lipids constitute the unit cell with TIP3P waters added at both sides. The system contains $MgCl_2$, KCl, $CaCl_2$, and $ZnCl_2$ at the same concentration of 25 mM to satisfy a total cations concentration near 100 mM. The CHARMM program[33] was used to construct the set of starting points and to relax the systems to a production-ready stage. Simulations of the initial construction and the pre-equilibration were performed on the NPAT (constant number of atoms, pressure, surface area, and temperature) ensemble. For production runs to 30 ns, the NAMD code[34] on a Biowulf cluster at the National Institutes of Health, Bethesda, MD (http://biowulf.nih.gov) was used for the starting point. In the production simulations, the dynamics were performed on both the NPAT and NPγT (constant number of atoms, pressure, surface tension, and temperature) ensembles with $\gamma = 0$. However, no significant differences in the critical results were found for the use of different ensembles. For each channel topology, three independent trajectories were produced, and averages were taken after 10 ns discarding initial transient.

(14) Ivanova, M. I.; Sawaya, M. R.; Gingery, M.; Attinger, A.; Eisenberg, D. *Proc. Natl. Acad. Sci. U.S.A.* **2004**, *101*, 10584–10589.
(15) Ivanova, M. I.; Thompson, M. J.; Eisenberg, D. *Proc. Natl. Acad. Sci. U.S.A.* **2006**, *103*, 4079–4082.
(16) Routledge, K. E.; Tartaglia, G. G.; Platt, G. W.; Vendruscolo, M.; Radford, S. E. *J. Mol. Biol.* **2009**, *389*, 776–786.
(17) Hirakura, Y.; Kagan, B. L. *Amyloid* **2001**, *8*, 94–100.
(18) Quist, A.; Doudevski, I.; Lin, H.; Azimova, R.; Ng, D.; Frangione, B.; Kagan, B.; Ghiso, J.; Lal, R. *Proc. Natl. Acad. Sci. U.S.A.* **2005**, *102*, 10427–10432.
(19) Kozhukh, G. V.; Hagihara, Y.; Kawakami, T.; Hasegawa, K.; Naiki, H.; Goto, Y. *J. Biol. Chem.* **2002**, *277*, 1310–1315.
(20) Ohhashi, Y.; Hasegawa, K.; Naiki, H.; Goto, Y. *J. Biol. Chem.* **2004**, *279*, 10814–10821.
(21) Yamaguchi, K.; Takahashi, S.; Kawai, T.; Naiki, H.; Goto, Y. *J. Mol. Biol.* **2005**, *352*, 952–960.
(22) Iwata, K.; Fujiwara, T.; Matsuki, Y.; Akutsu, H.; Takahashi, S.; Naiki, H.; Goto, Y. *Proc. Natl. Acad. Sci. U.S.A.* **2006**, *103*, 18119–18124.
(23) Zheng, J.; Ma, B.; Nussinov, R. *Phys. Biol.* **2006**, *3*, 1–4.
(24) Luhrs, T.; Ritter, C.; Adrian, M.; Riek-Loher, D.; Bohrmann, B.; Dobeli, H.; Schubert, D.; Riek, R. *Proc. Natl. Acad. Sci. U.S.A.* **2005**, *102*, 17342–17347.
(25) Petkova, A. T.; Yau, W. M.; Tycko, R. *Biochemistry* **2006**, *45*, 498–512.
(26) Ferguson, N.; Becker, J.; Tidow, H.; Tremmel, S.; Sharpe, T. D.; Krause, G.; Flinders, J.; Petrovich, M.; Berriman, J.; Oschkinat, H.; Fersht, A. R. *Proc. Natl. Acad. Sci. U.S.A.* **2006**, *103*, 16248–16253.
(27) Zheng, J.; Jang, H.; Nussinov, R. *Biochemistry* **2008**, *47*, 2497–2509.
(28) Liang, C.; Derreumaux, P.; Wei, G. *Biophys. J.* **2007**, *93*, 3353–3362.
(29) Liang, C.; Derreumaux, P.; Mousseau, N.; Wei, G. *Biophys. J.* **2008**, *95*, 510–517.
(30) Ma, B.; Nussinov, R. *Proc. Natl. Acad. Sci. U.S.A.* **2002**, *99*, 14126–14131.
(31) Jang, H.; Zheng, J.; Nussinov, R. *Biophys. J.* **2007**, *93*, 1938–1949.
(32) Jang, H.; Zheng, J.; Lal, R.; Nussinov, R. *Trends Biochem. Sci.* **2008**, *33*, 91–100.
(33) Brooks, B. R.; Bruccoleri, R. E.; Olafson, B. D.; States, D. J.; Swaminathan, S.; Karplus, M. *J. Comput. Chem.* **1983**, *4*, 187–217.
(34) Phillips, J. C.; Braun, R.; Wang, W.; Gumbart, J.; Tajkhorshid, E.; Villa, E.; Chipot, C.; Skeel, R. D.; Kale, L.; Schulten, K. *J. Comput. Chem.* **2005**, *26*, 1781–1802.

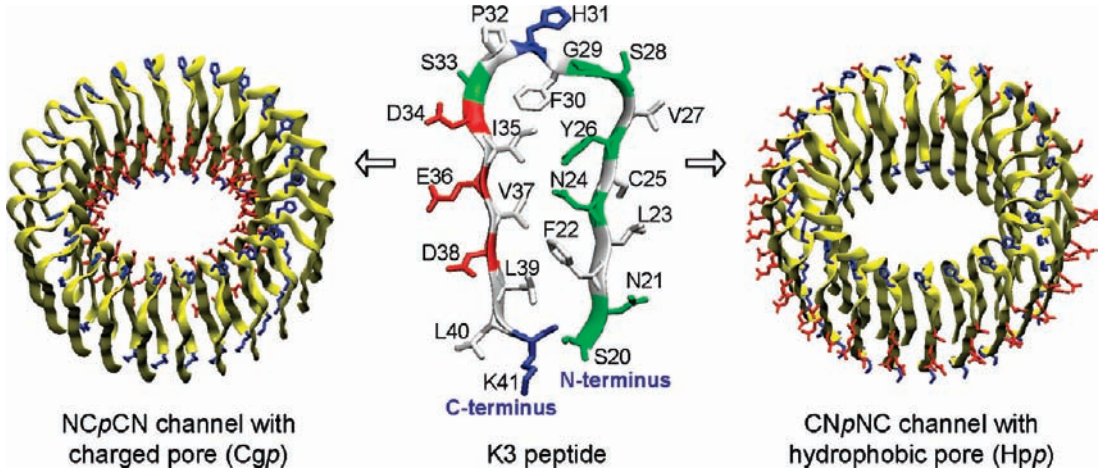

Figure 1. Building annular channel structures for the NC*p*CN channel with charged pore (Cg*p*) (left) and the CN*p*NC channel with hydrophobic pore (Hp*p*) (right) in the membrane by using the NMR-based K3 peptide. In the middle, the K3 peptide is shown in a ribbon representation. Hydrophobic residues are white, five polar (Ser20, Asn21, Asn24, Tyr26, Ser28, and Ser33) and Gly29 residues are shown in green, two positively charged residues (His31 and Lys41) are blue, and three negatively charged residues (Asp34, Glu36 and Asp38) are shown in red. In the channels, the backbone of K3 peptides is shown in a yellow ribbon representation, and the charged side chains are highlighted by the same colors used in the NMR.

Sample Preparation for AFM Imaging. Samples were prepared following previously published protocols.[18,35] Briefly, DOPC dissolved in chloroform was vacuum-desiccated overnight. The peptide solution, diluted in PBS, was used to hydrate the lipid to concentrations of 300−500 μg/mL. This was followed by 15 min vortexing and 20−30 min sonication in an ice−water bath at ∼4 °C. A 50 μL droplet of a solution of peptides reconstituted in liposomes was allowed to adsorb for 20−30 min on freshly cleaved mica to create a supported lipid bilayer with incorporated peptides. The sample was rinsed 3 times with PBS to eliminate all unincorporated peptides as well as liposomes that were not ruptured.

For imaging peptides on mica, a 1 mg/mL aliquot was sonicated in the ice−water bath for 20−30 min. PBS was added to a final concentration of 400 μg/mL. A 50 μL droplet of this solution was then deposited on mica and imaged after a few minutes.

AFM Imaging and Image Analysis. AFM images were acquired using a 5.30 Nanoscope controller with an Extender electronics module (Veeco, Santa Barbara, CA). Oxide-sharpened silicon nitride cantilevers with nominal spring constants (k_n) of 0.12 N/m (Veeco, Santa Barbara, CA) were used to image K3 peptides on mica. TR400PB Olympus cantilevers (Asylum Research, Santa Barbara, CA) with $k_n = 0.02$ N/m were used for imaging K3 reconstituted in lipid bilayers. Images were acquired in tapping mode at scan frequencies of 0.5−1.5 Hz and drive amplitudes below 100 mV. The cantilever oscillation frequency was 5−10 Hz. All scans were performed in PBS at room temperature using a fluid cell from Veeco.

Image analysis was performed using the Veeco software.[18] Some AFM images were low-pass filtered to remove noise. Sizes of the reconstituted channels in the membrane were obtained from the height images using cross-sectional analysis. Channel diameters were measured at two-thirds full height with respect to the lipid bilayer surface.

Formation of Planar Lipid Bilayers. To generate vertical planar lipid bilayers, we employed the "painting technique",[36] where a solution of lipids in heptane was applied over a small pore in the bilayer chamber. We used bilayer-cups with a pore diameter of ∼250 μm in a Delrin septum (Warner Instruments, Delrin perfusion cup, volume 1 mL) pretreated with the same lipid mixture dissolved in hexane. Bilayer membranes were made with a 1:1 (w/w) mixture of lipids POPG/POPE or DOPS/POPE dissolved in *n*-heptane.[37] The total lipid concentration of these solutions in heptane was 10−20 mg/mL.[38] As electrolyte we used 150 mM KCl with or without 10 mM Hepes pH 7.4. For ion selectivity experiments, we used DOPS/POPE (1:1) bilayers, with asymmetric KCl solutions, 44 mM in the trans side (ground) and 555 mM the cis side (hot wire), with symmetrically 4.5 mM Hepes pH 7.4 and 0.45 mM $MgCl_2$.

Current Recordings. Prior to painting, electrode asymmetry was verified to be less than 1 mV. For experiments, we chose membranes that were: stable in ±100 mV range for 10 min, with capacitances higher than 100 pF (typically ∼150 pF), and membrane conductances lower than 10 pS. Subsequently, we added 2−20 μL of K3 peptide into the *cis* side (hotwire) leading to a final K3 concentration of 0.8−8 μM in the bilayer-chamber. Mixing was obtained by stirring the chamber for 1−2 min. We performed all recordings using an EPC-7 amplifier set in "voltage clamp mode" with a gain set at 10 mV/pA using Ag/AgCl electrodes. We used the filter-cutoff frequency of 3 kHz. Data acquisition recordings were done using custom-made software. Sampling frequency was set at 15 kHz for all bilayer experiments. For representation in figures, we filtered the current versus time traces with a digital Gaussian low-pass filter at a cutoff frequency of 100 Hz.

Cell Culture. Human Kidney Proximal Tubule cells (HK2) were cultured following ATCC's recommendations. Cells were split 48 h before the experiment and seeded at low densities (∼5000 cells/cm^2). Cells were loaded with the Fluo-4 NW calcium sensitive dye following the manufacturer's recommended protocol.

Fluorescence Imaging and Data Analysis. Molecular Probes Fluo-4 NW calcium assay kit was used to monitor the calcium changes within the cell. Cells were loaded with the dye following manufacturer's recommended protocol. Typically, cells were washed free of serum proteins in the assay buffer (HBSS buffer). Five-hundred microliters of dye mixed with 2.5 mM probenecid was added to each well and incubated for 45 min at 37 °C. For the experiments of Ca^{2+} uptake inhibition, 50 μM $ZnCl_2$ previously solubilized in HBSS was added to the dye and incubated with the cells for 40−45 min.

Cells were transferred to the onstage incubator system (20/20 Technologies, USA) mounted on an inverted optical microscope

(35) Lin, H.; Bhatia, R.; Lal, R. *Faseb J.* **2001**, *15*, 2433–2444.
(36) Mueller, P.; Rudin, D. O.; Tien, H. T.; Wescott, W. C. *Nature* **1962**, *194*, 979–980.
(37) Capone, R.; Blake, S.; Restrepo, M. R.; Yang, J.; Mayer, M. *J. Am. Chem. Soc.* **2007**, *129*, 9737–9745.
(38) Capone, R.; Garcia Quiroz, F.; Prangkio, P.; Sauer, A. M.; Bautista, M. R.; Turner, R. S.; Yang, J.; Mayer, M. *Neurotox. Res.* **2009**, *16*, 1–13.

(Olympus IX71) equipped with FITC filter set (Ex/Em: 480/536 nm, Semrock). Ratio imaging (F_t/F_0, see below for details) was carried out with RatioPlus module of IPLab (BD Biosciences) software. A random field was chosen and an image was acquired. This image was segmented interactively to separate the cells as blobs to use as a mask for analysis. Blobs are individual cells, groups of cells, particles or an ROI in the segmented image. Cell debris (particles) was excluded from the analysis by interactive thresholding. The same field was imaged every 30 s for 45 min or more. Typically, first 2 frames were acquired to establish the baseline distribution of Ca^{2+}. K3 peptide was added (10 μM) to the buffer and imaging continued. Images were acquired with a 1024 × 1024 pixels monochrome camera (Cascade II, Photometrics) and stored as X,Y,T stacks for analysis.

A script was written in IPLab to interact with the RatioPlus module to plot the ratio of fluorescence change [(F_t/F_0)*100] with time for each blob. F_t is the calcium specific fluorescence of the blob at a given time 't' and F_0 is the fluorescence at time $t = 0$. An average fluorescence plot was generated for all the blobs in the field after careful elimination of blobs that include unhealthy cells and cells moved out of the mask during acquisition process. Several experiments were performed for each condition and their average plots were employed to compute the mean ratio of fluorescence for that condition. All experiments were done at 20× magnification.

Results

Modeling K3 Channels in the Lipid Bilayer. We modeled the K3 channels embedded in a DOPC bilayer using the ssNMR-based coordinates.[22] We modeled two channel configurations: NC*p*CN with charged pore (Cg*p*) and CN*p*NC with hydrophobic pore (Hp*p*) (Figure 1). The N-terminal β-strand of K3 contains mostly hydrophobic residues while the C-terminal strand includes three negatively charged residues (Asp34, Glu36, and Asp38). Two positively charged residues (His31 and Lys41) are located at each end of the longer molecular axis. In the Cg*p* channel, the negatively charged residues enclose the central pore while the hydrophobic residues make contact with the lipids, and *vice versa* in the Hp*p* channel. At $t > 5$ ns, the initial frustration in the annular conformation is gradually removed via lipid dynamics, and environmentally relaxed channel structures can be observed. The Cg*p* channels (Figure 2, left column) increase both the outer diameter and the inner pore sizes. In the starting conformation, the outer Cg*p* channel diameter is ~7.7 nm, and the pore diameter is ~2.4 nm. In the final Cg*p* channels, the outer and pore diameters are ~8.3−8.8 nm and ~2.7−3.2 nm, respectively. While in the Hp*p* channels (Figure 2, right column) the outer diameters increase to ~7.4−8.2 nm starting from ~7 nm, the pore diameter is greatly decreased to ~1.5−1.8 nm from ~2.2 nm. The Hp*p* channels yield collapsed hydrophobic pore. Both relaxed channels abandoned the perfect annular morphologies, breaking into several ordered subunits.[31,32] The Cg*p* channels obtain 5 to 6 subunits and the Hp*p* channels obtain 3 to 4 subunits, consistent with other amyloid[18,31,32,35] and other β-sheet channels.[39]

AFM Imaging. Earlier studies indicated that K3 can obtain a multitude of architectures, from globular oligomers to fibrils.[19,40,41] In our study, AFM was used to visualize the polymorphic K3 peptide assemblies. AFM images of freshly dissolved high concentration K3 peptides adsorbed on mica showed globular

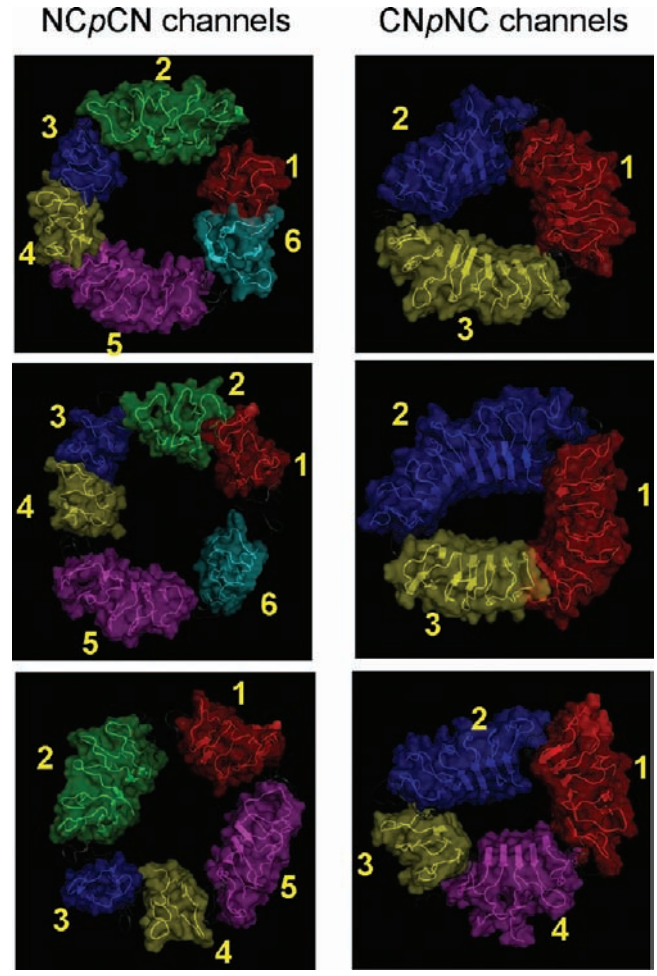

Figure 2. Simulated channel structures with highlighted subunits. The NC*p*CN channels (left column) with charged pore (Cg*p*) and CN*p*NC channels (right column) with hydrophobic pore (Hp*p*) are shown in the view along the membrane normal. For each channel topology, three different channel structures were obtained from three independent trajectories.

structures as well as fibrillar striated features (Figure 3A and B). The size of the globular structures ranged from 1.5 to 3 nm in height, in good agreement with previous results.[21,40,41]

K3 peptides reconstituted in DOPC bilayers present polymorphic structures at varying peptide to lipid ratios. At high ratios (1:5 by mass), a mixture of peptide fibrils and lipid bilayers was observed (Figure 3C, D). Higher resolution AFM images showed that the striation structure seen in (Figure 3A, B) was still present (Figure 3E, F). As the peptide to lipid ratio was decreased (1:30 by mass), fibrillar and annular structures were observed (Figure 3G, H). Fewer fibrils were observed at decreasing ratios, and only annular structures were recognized at ratios of ~1:50 (Figure 4). These doughnut-like structures, already described for other amyloids,[18,35] possess characteristics in good agreement with the predictions by the model presented above.

K3 peptides reconstituted in the DOPC bilayers show channel-like structures protruding out of the membrane plane. Higher resolution imaging showed subunit arrangement. Highlighted areas (Figure 4A) show circular structures with identifiable subunits. Representative channel-like structures are shown in the magnified images (Figure 4B−E) to emphasize the subunit organization. The plots (Figures 4F and 4G) show the range of the inner and outer pore diameters, respectively - inner diameters

(39) Jang, H.; Ma, B.; Lal, R.; Nussinov, R. *Biophys. J.* **2008**, *95*, 4631–4642.
(40) Ban, T.; Yamaguchi, K.; Goto, Y. *Acc. Chem. Res.* **2006**, *39*, 663–670.
(41) Ozawa, D.; Yagi, H.; Ban, T.; Kameda, A.; Kawakami, T.; Naiki, H.; Goto, Y. *J. Biol. Chem.* **2009**, *284*, 1009–1017.

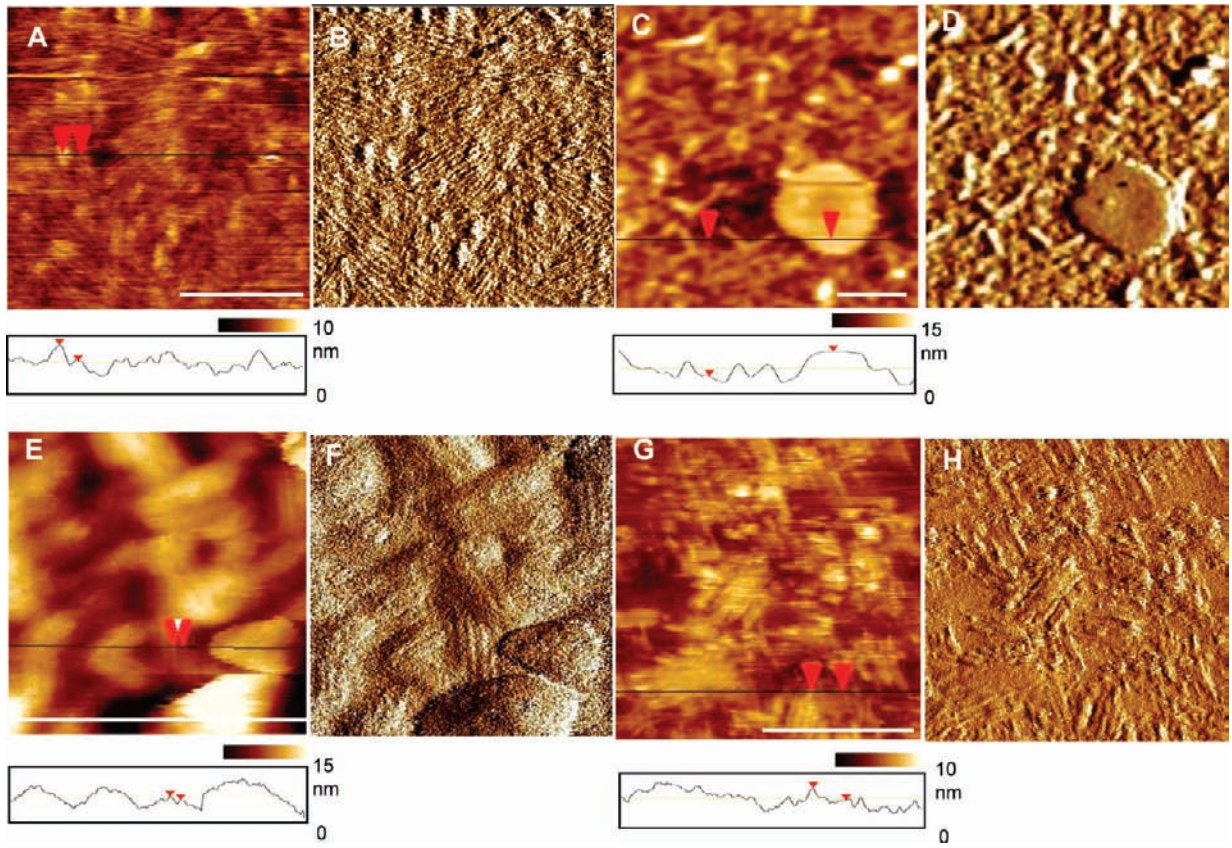

Figure 3. Tapping mode AFM images of K3 peptide in PBS adsorbed on mica. The height image and height profile are represented in (A). Cross sectional height profile corresponds to the black line marked in the image. Fibrillar striated structures are more clearly observed in the amplitude (error mode) image (B). (C−H) AFM images of K3 reconstituted in DOPC lipid bilayer. (C−F) Peptide/lipid ratio of 1:5 (by mass); (G) and (H) K3/DOPC mass ratio of 1:30. (C), (E), and (G) Height images and height profiles. (D), (F), and (H) Corresponding amplitude images. Scale bar is 200 nm for all images and it is displayed only for height images. Amplitude images have the same size as their corresponding height images for each peptide to lipid ratio.

∼2.6 nm and outer diameters ∼7.1 nm. The number of subunits ranged from 3 to 6 (Figure 4H) as predicted by the model. The majority of the structures have 3 subunits (∼40%), while ∼25% have 6 subunits. In order to determine if these pore-like structures have any ion channel-like activity, we measured electrical conductance using the planar lipid bilayer system (PLB).

Electrical Conductance Measurements. Figure 5 shows that reconstituted K3 peptides in the lipid bilayer have electrical conductance, consistent with the pore-like structures predicted by the modeling and observed in the AFM measurements. As with other amyloid peptides, K3 shows a multiconductance pore forming behavior (Figure 5A), similar to the full-length β_2m pore forming activity in artificial membranes[17] and other amyloid pores.[18,35,38,42−48] Like full-length β_2m, the K3 fragment displays open and closed states that are sustained in the seconds to minutes range (Figure 5B). We tested the K3 membrane behavior in the concentration range between 0.8 μM to 8 μM by directly adding the peptide to one side of the bilayer chamber. In this concentration range, we observed K3 activity consistent with the results presented in Figure 5 in more than 90% of all trials. We tested this activity in two anionic lipid mixtures, (POPG/POPE and DOPS/POPE). In the POPG/POPE membranes K3 channels can be in a flickering state that seems to be stable for minutes (data not shown). Ion selectivity experiments showed weak cation selectivity ($P_K/P_{Cl} \approx 5 \pm 0.7$, $n = 3$), suggesting an excess of negatively charged groups in or near the pore. This selectivity value is in agreement with a charged pore model structure as presented in this study. Additionally, we observe that K3 pore activity is inhibited by Zn^{2+} ions, like other amyloid channels.

While AFM imaging and MD simulations were performed in DOPC bilayers, PLB recording measurements were carried out in mixtures including anionic lipids. The choice of the lipids for the structural and electrophysiological studies primarily reflects the experimental constraints of the techniques.[18] For electrophysiolgical studies, we used anionic lipids to facilitate K3 binding to the preformed bilayer surface and subsequent entry into the lipid core where the K3 peptides assemble into electrically conducting form(s). It has been observed that several amyloids interact preferably with anionic membranes[49−53] and

(42) Kagan, B. L.; Azimov, R.; Azimova, R. *J. Membr. Biol.* **2004**, *202*, 1–10.
(43) Arispe, N. *J. Membr. Biol.* **2004**, *197*, 33–48.
(44) Arispe, N.; Rojas, E.; Pollard, H. B. *Proc. Natl. Acad. Sci. U.S.A.* **1993**, *90*, 567–571.
(45) Bhatia, R.; Lin, H.; Lal, R. *Faseb J.* **2000**, *14*, 1233–1243.
(46) Lal, R.; Lin, H.; Quist, A. P. *Biochim. Biophys. Acta* **2007**, *1768*, 1966–1975.
(47) Lin, M. C.; Kagan, B. L. *Peptides* **2002**, *23*, 1215–1228.
(48) Mirzabekov, T. A.; Lin, M. C.; Kagan, B. L. *J. Biol. Chem.* **1996**, *271*, 1988–1992.
(49) Wong, P. T.; Schauerte, J. A.; Wisser, K. C.; Ding, H.; Lee, E. L.; Steel, D. G.; Gafni, A. *J. Mol. Biol.* **2009**, *386*, 81–96.

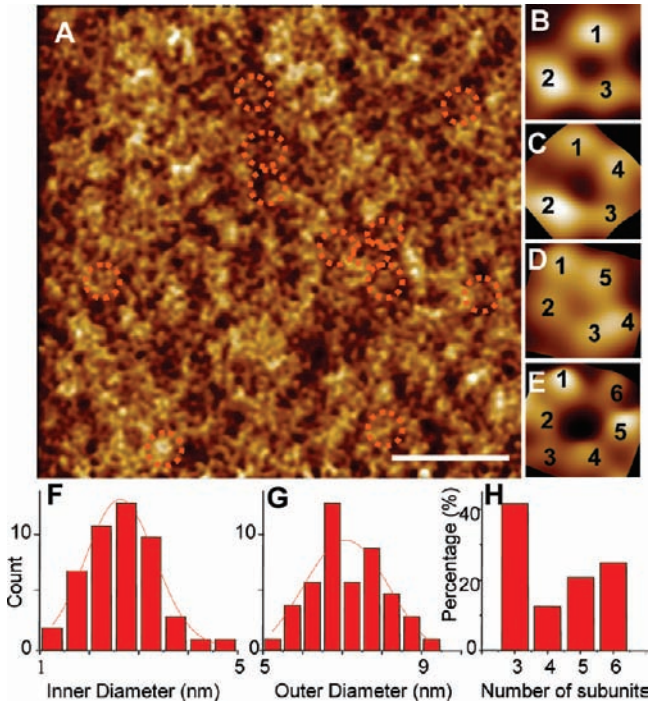

Figure 4. (A) AFM images in tapping mode of K3 peptide reconstituted in DOPC lipid bilayer at a 1:50 (mass ratio) peptide to lipid ratio. Pore-like structures similar to the ion channels predicted by the MD simulations are enclosed by dotted circles. The pore-like structures had 3−6 subunits, as shown in the magnified images of the selected areas (B−E). Cross section analysis reveals the pore size to take average values of 2.6 nm for the inner diameter and 7.2 nm for the outer diameter. The ion channel dimensions were analyzed by fitting the size distributions to Gaussian curves with centroids at 2.62 nm for the outer diameter (F) and 7.09 nm for the outer diameter (G). The distribution for the number of subunits is displayed in (H).

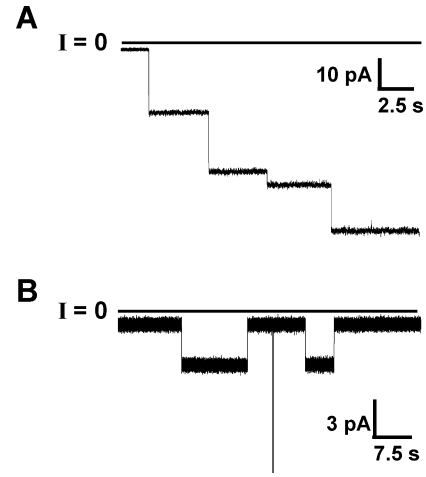

Figure 5. K3 peptide has pore forming activity in artificial membranes. (A) Example of K3 multiconductance current steps at a final concentration of 1 μM. (B) Example of long-lived opening and closure of K3 pore at 1 μM. Both recordings were performed at an applied potential of −40 mV. The vertical line in panel (B) is a single spike with opening time of 100 ms and amplitude of 20 pA. Membranes were prepared from lipid mixtures of DOPS/POPE dissolved in heptane at a 1:1 (w/w) ratio by the "painted method" over a 250 μm pore in a Delrin bilayer cup that was pretreated with same lipids in hexane. We used 150 mM KCl, 1 mM $MgCl_2$ and 10 Hepes, pH 7.4 as electrolyte. For more experimental details, see the Materials and Methods section.

no binding is obtained in fluid PC bilayers[54] unless a particular procedure is used.[55] For AFM studies, amyloids are mixed with liposomes in solution wherein the insertion of amyloids into the membrane is thermodynamically appropriate even for a neutral lipid. On the other hand, having highly purified lipids in the bilayer helps distinguish proteins structures from lipids more efficiently.[18,56]

The conductance measurements presented here are in agreement with previous work of Hirakura and Kagan,[17] and the multiple single channel conductances observed for K3 suggest that the subunits may arrange to form a range of channel structures. This is in agreement with the model proposed here and the AFM measurements. With this in mind, we designed experiments aimed at understanding if the K3 fragment would be toxic to cells.

K3 Alters Calcium Flux in Cells. Consistent with MD simulations, AFM imaging demonstrated that K3 forms pore like structures and conductance measurements showed that K3 permeates ions across the bilayer. To correlate the pore activity with pathogenicity, we examined the effect of K3 on cell calcium homeostasis, since regulation of intracellular calcium is tightly linked with cell stress and death.[57−60] Calcium specific fluorescence was measured before and after adding K3 (10 μM) in normal Ca^{2+} medium. The results showed a fast increase in fluorescence in the first 25 min followed by a slow increase for the next 20 min, to a total fluorescence increase of about 8% from the basal level (Figure 6). On the other hand, the control experiment used identical volume of vehicle (1% NH_4OH) and showed only 1% increase in fluorescence. Pretreating the cells with zinc shows an inhibition in Ca^{2+} uptake with an increase in fluorescence of only 2% after 45 min. This finding is consistent with the electrical recording in bilayer membrane prediction that the pore activity is inhibited by Zn^{2+} ions. The measured intracellular Ca^{2+} increase, combined with the electri-

(50) Chauhan, A.; Ray, I.; Chauhan, V. P. *Neurochem. Res.* **2000**, *25*, 423–429.
(51) Zhao, H.; Tuominen, E. K.; Kinnunen, P. K. *Biochemistry* **2004**, *43*, 10302–10307.
(52) Jayasinghe, S. A.; Langen, R. *Biochemistry* **2005**, *44*, 12113–12119.
(53) Maltseva, E.; Kerth, A.; Blume, A.; Mohwald, H.; Brezesinski, G. *Chembiochem* **2005**, *6*, 1817–1824.
(54) Yoda, M.; Miura, T.; Takeuchi, H. *Biochem. Biophys. Res. Commun.* **2008**, *376*, 56–59.
(55) de Planque, M. R.; Raussens, V.; Contera, S. A.; Rijkers, D. T.; Liskamp, R. M.; Ruysschaert, J. M.; Ryan, J. F.; Separovic, F.; Watts, A. *J. Mol. Biol.* **2007**, *368*, 982–997.
(56) Lin, H.; Zhu, Y. J.; Lal, R. *Biochemistry* **1999**, *38*, 11189–11196.
(57) Bezprozvanny, I.; Mattson, M. P. *Trends Neurosci* **2008**, *31*, 454–463.
(58) Mattson, M. P.; Chan, S. L. *Nat. Cell Biol.* **2003**, *5*, 1041–1043.
(59) Schanne, F. A.; Kane, A. B.; Young, E. E.; Farber, J. L. *Science* **1979**, *206*, 700–702.
(60) Trump, B. F.; Berezesky, I. K. *Faseb J.* **1995**, *9*, 219–228.
(61) Argiles, A.; Garcia-Garcia, M.; Derancourt, J.; Mourad, G.; Demaille, J. G. *Kidney Int.* **1995**, *48*, 1397–1405.
(62) Bellotti, V.; Stoppini, M.; Mangione, P.; Sunde, M.; Robinson, C.; Asti, L.; Brancaccio, D.; Ferri, G. *Eur. J. Biochem.* **1998**, *258*, 61–67.
(63) Heegaard, N. H. H.; Jorgensen, T. J. D.; Rozlosnik, N.; Corlin, D. B.; Pedersen, J. S.; Tempesta, A. G.; Roepstorff, P.; Bauer, R.; Nissen, M. H. *Biochemistry* **2005**, *44*, 4397–4407.
(64) Linke, R. P.; Bommer, J.; Ritz, E.; Waldherr, R.; Eulitz, M. *Biochem. Biophys. Res. Commun.* **1986**, *136*, 665–671.
(65) Linke, R. P.; Kerling, A.; Rail, A. *Kidney Int. Suppl.* **1993**, *41*, S100–105.
(66) Vincent, C.; Dennoroy, L.; Revillard, J. P. *Biochem. J.* **1994**, *298*, 181–187.

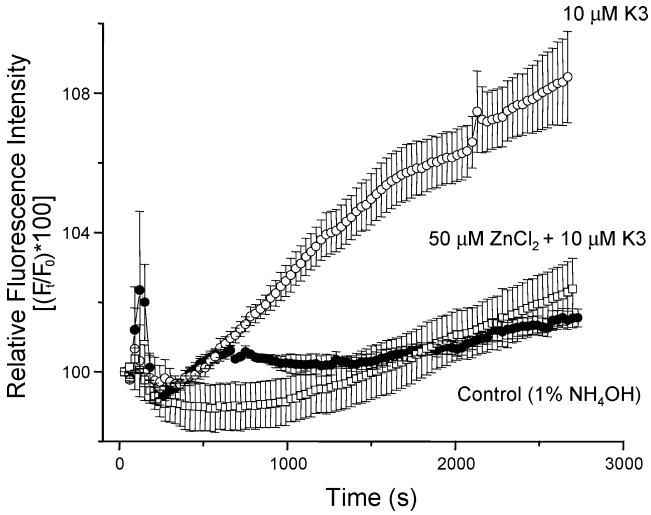

Figure 6. Calcium uptake monitored by Fluo-4 NW dye in human kidney cells. Cells treated with K3 (10 μM) showed a significant increase in calcium specific fluorescence compared to its control treated with 1% ammonium hydroxide solvent alone. Pretreatment with 50 μM $ZnCl_2$ shows a decreased uptake of Ca^{2+} when the same amount (10 μM) of K3 was added. The plots show the percentage increase in fluorescence $(F_t/F_0)*100$ against time, where F_t is the fluorescence intensity at time 't' and F_0 is the fluorescence intensity of the field at $t = 0$. The error bars represent the standard deviation of multiple experiments.

cal recording in bilayer membrane suggests that K3 forms conductive pores with predilection to cation(s).

Discussion

Apart from the large amount of β_2m fibrils, amyloid plaques isolated from DRA patients contain proteolytic β_2m fragments.[5,6,11,61−66] These fragments can act as seeds accelerating amyloid aggregation.[11,12,14] Consequently, a study of a proteolytic fragment earlier shown to fibrillate in membranes is important to the understanding of DRA. Our combined data strongly suggest that when embedded in the membrane, K3 (a 22-residue β_2m fragment) creates a functional ion channel-like structure. These data are in agreement with the modeled K3 channel based on the ssNMR *β-strand-turn-β-strand* motif.[22] The initial constructed model is perfectly annular; however, in the simulations the channels break into 3 to 6 loosely attached, mobile subunits, where each subunit is composed of several monomers. AFM measurements revealed pore-like structures with dimensions in agreement with the model predictions: average inner pore diameter ∼2.6 nm; outer diameter ∼7.1 nm. Pores predominantly composed of 3 subunits were clearly identified in AFM images. We further observed a gradual change in the surface density of thin fibrils on mica to annular structures incorporated into DOPC bilayers depending on the peptide to lipid ratio. Polymorphic coexistence of both structures was also possible expanding earlier fibril formation results.[21] We speculate that the *β-strand-turn-β-strand* motif that appears to favor annular structures at low peptide to lipid ratios may favor different K3 fibril states at different ratios.

It is expected that the CN*p*NC topology (hydrophobic pore) would be unstable and short-lived due to the unfavorable interaction between the charged amino acids at the outer β-stands and the hydrophobic core of the membrane. This structure either collapses or evolves and rearranges depending on the lipid headgroups into another more stable toroidal pore. Using AFM imaging, we observed a distribution of pores composed of 3−6 subunits, in agreement with the modeled predictions. However, the AFM experimental design was such that we could not distinguish hydrophobic vs hydrophilic pore as defined in the models for the CN*p*NC or NC*p*CN topologies of the channel organizations. This issue will be addressed in future studies using suitable AFM experimental paradigm.[67]

The annular structures observed in AFM images suggest that the central cavity spans across the thickness of the lipid bilayer. However, due to the relative large size of the AFM tip (pyramidal in shape with >5 nm tip radius at the apex) compared to the K3 pore size (<3 nm in diameter), AFM provides information only about depths in the proximity of the lipid bilayer/solution interface and cannot discern whether the annular structures are conducting or not. We applied electrophysiological measurements to evaluate the functional status of these pores in planar lipid bilayers. The conductance measurements presented here are in agreement with the previous work of Hirakura and Kagan, 2001,[17] suggesting that K3 could be the pore forming element of β_2m. Nonetheless, our results do not exclude the possibility that other β_2m fragments also have similar abilities. These results, together with the K3 ability to form fibrils in solution,[21] and on membranes (as demonstrated above) suggest that the K3 sequence has fibril and pore forming properties. The multiple single channel conductances for K3 suggest that different number of subunits can dynamically associate/dissociate to form labile pore structures, in agreement with AFM measurements and modeling predictions.

Conclusions

To conclude, here we have presented the first study providing atomic scale modeling of K3 amyloid channel in the bilayer, combined with comprehensive experimental analysis by AFM, single channel electrical recording, and fluorescence imaging of calcium uptake. Together, these provide compelling data substantiating channel formation by K3. Significantly, K3 pores altered the calcium flux in human kidney cells. These findings are in good correlation with other amyloid channels that allow calcium uptake.[68,69] The proteolytic β_2m fragment K3 is also able to form fibrils[21] in addition to ion permeable pores in membranes. This feature is similar to that of other amyloids,[18,35,43−49,70] suggesting that K3 could be the pore forming element of β_2m.[17] Fragment effects (on cell/membrane) have also been observed.[71−73] Further, ssNMR illustrates that K3 oligomers present the *β-strand-turn-β-strand* motif. Recently accumulating experimental evidence from various amyloids has shown that the *β-strand-turn-β-strand* motif is universal in amyloids, suggesting that these channels may also be generic. However, as in protein folding, channel details will vary,

(67) Thimm, J.; Mechler, A.; Lin, H.; Rhee, S.; Lal, R. *J. Biol. Chem.* **2005**, *280*, 10646–10654.
(68) Demuro, A.; Mina, E.; Kayed, R.; Milton, S. C.; Parker, I.; Glabe, C. G. *J. Biol. Chem.* **2005**, *280*, 17294–17300.
(69) Kawahara, M.; Kuroda, Y.; Arispe, N.; Rojas, E. *J. Biol. Chem.* **2000**, *275*, 14077–14083.
(70) Brender, J. R.; Hartman, K.; Reid, K. R.; Kennedy, R. T.; Ramamoorthy, A. *Biochemistry* **2008**, *47*, 12680–12688.
(71) Rhoades, E.; Gafni, A. *Biophys. J.* **2003**, *84*, 3480–3487.
(72) Brender, J. R.; Lee, E. L.; Cavitt, M. A.; Gafni, A.; Steel, D. G.; Ramamoorthy, A. *J. Am. Chem. Soc.* **2008**, *130*, 6424–6429.
(73) Brender, J. R.; Durr, U. H.; Heyl, D.; Budarapu, M. B.; Ramamoorthy, A. *Biochim. Biophys. Acta* **2007**, *1768*, 2026–2029.

depending on the sequences and the environment, for example, membrane composition. A charged sequence facing the bilayer is expected to lead to a toroidal channel; hydrophobic outward facing residues are likely to form a barrel-stave channel. Nonetheless, the mobile subunit organization in the fluidic membrane is expected to be universal.

Acknowledgment. This project has been funded by the National Cancer Institute, National Institutes of Health, under contract No. N01-CO-12400, by the Intramural Research Program of the National Institutes of Health, National Cancer Institute, Center for Cancer Research. R.L. acknowledges support from the NIH (NIA) extramural program. H.J. did the modeling; M.M. and F.T.A. contributed to AFM experiments; R.C. did the electrophysiology; S.R. and M.M. contributed to cell work. This study utilized the high-performance computational capabilities of the Biowulf PC/Linux cluster at the National Institutes of Health, Bethesda, MD (http://biowulf.nih.gov).

JA9049299